Artifact-free T2* mapping without post hoc corrections

Pippa Storey[1], Yvonne W. Lui[1], and Dmitry S. Novikov[1]
[1]*Radiology Department, New York University School of Medicine, New York, NY, United States*

Introduction: T2* mapping is widely performed in the brain and body for tissue iron quantification and blood oxygenation level dependent (BOLD) imaging. It exploits the fact that paramagnetic molecules such as ferritin, hemosiderin and deoxyhemoglobin generate magnetic field inhomogeneities on a mesoscopic (cellular) scale, which cause signal dephasing and T2* shortening. However, macroscopic susceptibility differences, due for example to air in the sinuses or bowel, produce magnetic field gradients across whole voxels, which also result in dephasing. Various post hoc correction methods have been proposed, but are often cumbersome [1] or inaccurate, ignoring the point-spread function in the Fourier-encoded directions and the slice profile in 2D imaging [2]. Here we show that Fourier encoding is largely insensitive to macroscopic phase gradients up to a threshold determined by the Nyquist limit. Accurate T2* maps can be thus obtained without post hoc correction simply by acquiring data in 3D mode and truncating the echo train where the local phase gradient exceeds the threshold. We also show that the use of a Hann filter to suppress point spread effects [1] exacerbates sensitivity to macroscopic field gradients, but that a Tukey filter offers a favorable alternative.

Methods: Phantom and human studies were performed at 3T (Siemens Tim Trio and Skyra respectively). A standard doped cylindrical phantom was placed in a CP coil with its long axis aligned with the bore. It was imaged in the presence of a wire, which was oriented parallel to the phantom and used to create macroscopic magnetic field gradients primarily in the transverse plane (Fig 1). 3D and multislice 2D multiple gradient echo (MGRE) acquisitions were each performed in axial and coronal planes with isotropic 2mm resolution and 32 monopolar echoes (TE = 2.50 – 71.94 ms). In the human study, 3 women (aged 24 – 55) were scanned using a 20-channel head coil. 3D and multislice 2D MGRE images of the brain were collected with isotropic 2mm resolution and 28 monopolar echoes (TE = 2.25 – 77.85 ms).

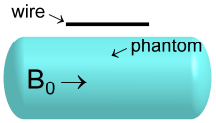

Fig. 1: Phantom setup.

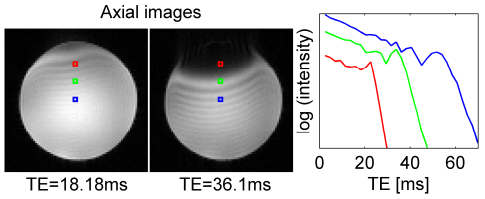

Fig. 2: Axial 3D phantom images at two echo times and signal decay on a semilog scale from pixels shown.

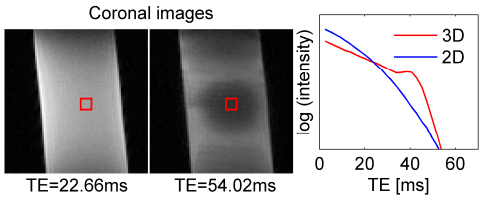

Fig. 3: Coronal 3D images at two echo times and signal decay from matched ROIs in 3D and 2D acquisitions.

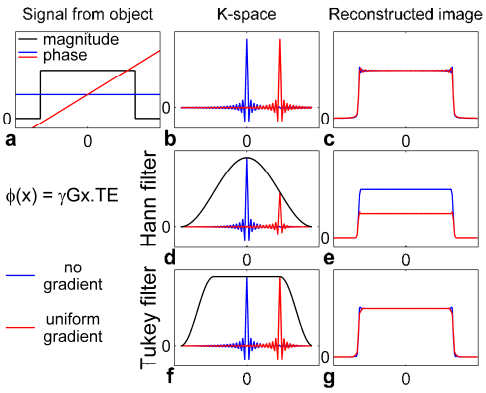

Fig. 4: Effect of a magnetic field gradient on Fourier encoded signal without (b-c) and with (d-g) filters.

Discussion: We have offered a simple prescription for accurate T2* mapping without post hoc corrections based on a 3D MGRE acquisition. In situations such as breath-hold imaging where 2D imaging is chosen due to time constraints, corrections for macroscopic dephasing need be applied only in the slice direction.

References: [1] MRM 70: 1283 (2013) [2] MRM 55: 1350 (2006) **Grants:** NIH NS039135 and P41 EB017183

Results: On the 3D phantom images, the wire produced intensity oscillations and signal loss, which increased with TE (Fig 2). For each voxel, the signal exhibited an initial monoexponential decay, followed by oscillations of increasing amplitude, and finally a precipitous decline. However, the time constant of the initial decay was similar for all voxels, suggesting that it represented the true T2* value. In the coronal acquisitions (Fig 3), the field gradient due to the wire was primarily in the through-plane direction. The 3D signal exhibited the same features as in the axial plane, while the decay of the 2D signal was nonexponential and more rapid, reflecting the influence of macroscopic field gradients over the slice profile. This demonstrates the benefit of Fourier encoding in all three directions. To understand this benefit, consider the simple case of a uniform gradient along a single dimension (Fig 4). The field gradient G produces a linear phase shift $\varphi(x) = \gamma Gx.TE$ across the object (Fig 4a). This phase modulation corresponds to a displacement in k-space (Fig 4b). Provided the phase difference between adjacent voxels is substantially less than π, the echo is still adequately captured, and the intensity of the image is not significantly reduced (Fig 4c). With increasing TE, however, the edges and finally the center of the echo will move outside the sampled region of k-space, producing intensity oscillations followed by a sudden drop in signal, as observed in Figure 2. The oscillations can be eliminated by applying a filter (Fig 5). However, the commonly used Hann window alters the signal decay, making it nonexponential and more rapid (Fig 5). The reason is that the Hann filter reduces the amplitude of the shifted echo (Fig 4). A preferable alternative is the Tukey filter, which preserves the amplitude of the shifted echo over most of the useful range (Fig 4), thus maintaining the correct rate of signal decay without oscillations (Fig 5). To calculate T2* for each voxel, we truncated the echo train at the TE value for which the phase difference from adjacent voxels in any direction exceeded απ, where α was chosen empirically to be 0.4. With this approach, the unfiltered 3D and Tukey-filtered 3D data produced uniform T2* maps in the phantom (Fig 6), demonstrating robustness to macroscopic effects. The 2D and Hann-windowed 3D data, however, produced anomalously short T2* values (Fig 6). Unfiltered 3D data also performed better than 2D in vivo near the sinuses (Fig 7).

Fig. 5: Axial phantom images in the absence and presence of filters, and the effect of those filters on signal decay in the pixel indicated.

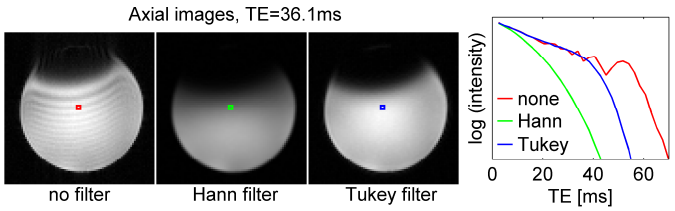

Fig. 6: T2* maps of the phantom from 2D and 3D acquisitions without and with filters. The unfiltered 3D and Tukey-filtered 3D data are very robust to macroscopic susceptibility.

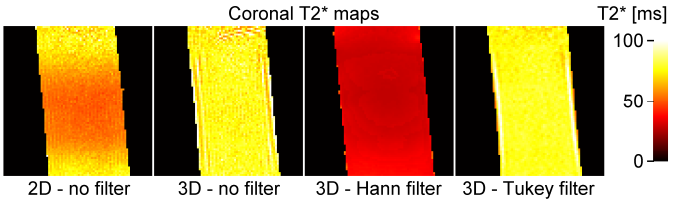

Fig. 7: Axial images of a 55-year old woman at two echo times and T2* maps from 2D and 3D acquisitions of the same slice. The susceptibility artifact on the 2D map above the paranasal sinuses is absent on the 3D map.